

# **APPLICATION OF PHOTOTHERMAL AND PHOTOACOUSTIC SPECTROSCOPY FOR THE MONITORING OF AQUEOUS DISPERSIONS OF CARBON NANOMATERIALS**

Authors:

D.S. Volkov, M.A. Proskurnin, I.V. Mikheev, D.V. Vasil'ev, M.V.  
Korobov, D.A. Nedosekin, V.P. Zharov

DOI: 10.12684/alt.1.94

Corresponding author: D.S. Volkov  
e-mail: dmsvolkov@gmail.com

---

# Application of Photothermal and Photoacoustic Spectroscopy for the Monitoring of Aqueous Dispersions of Carbon Nanomaterials

D.S. Volkov<sup>1</sup>, M.A. Proskurnin<sup>1</sup>, I.V. Mikheev<sup>1</sup>, D.V. Vasil'ev<sup>1</sup>, M.V. Korobov<sup>1</sup>,  
D.A. Nedosekin<sup>2</sup>, V.P. Zharov<sup>2</sup>

<sup>1</sup>Analytical Chemistry Division, Chemistry Department, Lomonosov Moscow State University, Moscow, 119991, Russia

<sup>2</sup>Philips Classic Laser Laboratories, University of Arkansas for Medical Sciences, Little Rock, Arkansas, 72205, USA

## Abstract

Photothermal and optoacoustic spectroscopy in their state-of-the-art techniques—multiwavelength, scanning and transient—are used for complex investigation and analysis (chemical analysis and the estimation of physicochemical properties and size) of novel carbon materials—fullerenes and nanodiamonds—and their aqueous dispersions as promising biomedical nanosystems. The estimation of the cluster size and the possibilities to determine subnanogram amounts of both nanodiamonds and fullerenes by these techniques are shown. The comparison of fullerene solutions in various solvents, toluene, N-methylpyrrolidone and water, is made. The advantages of the photothermal and optoacoustic techniques over conventional spectroscopies and the current limitation are discussed. The necessity to develop robust models for transient and imaging photothermal techniques is outlined.

## Introduction

Unique properties of new allotropic forms of carbon—fullerenes, nanotubes, and nanodiamonds (NDs)—find various applications in state-of-the-art branches of science and technology. They are used in the formation of composites, electronic instruments, and catalysts. They are promising for biomedical applications [1], catalysis [2, 3], and as new sorbents [4-7]. They can be used as fluorescent and contrast agents [8-10] in clinical diagnostics, as platforms for drug delivery [11, 12], as enterosorbents, diagnostic sensors, in cellular surgery, anticancer therapy, and many other areas [1]. ND biocompatibility has been insensitively investigated recently [13]. Low ND and fullerene toxicity was shown for neurons [14] stem cells [15], pulmonary epithelium [16, 17], blood cells [18], fibroblasts [16, 17], ovary tissues [19] etc.

As the biological properties of colloid solutions of fullerenes depend on the size of fullerene aggregates [20], it is necessary to control this

parameter. The methods used for this, dynamic light scattering (DLS) and low-angle neutron scattering have some significant drawbacks like very complicated data-handling routines and the problem of scattering on large particles.

Thus, the aim of this work was to show is it possible to use photothermal (PT) and optoacoustic (OA) spectroscopies as state-of-the-art methods of molecular and supramolecular spectroscopy for estimating size and concentrational dependences in dispersions exemplified by nanodiamonds and fullerenes.

## Materials and Methods

### Thermal-lens spectrometer

The thermal-lens spectrometer used in the work to monitor the changes in the solution properties was developed on the base of the spectrometer [21] optimized for the determination of solutions with a light absorption down to  $1 \times 10^{-6}$  abs. units. The scheme is given at Fig. 1. The key parameters are summarized in Table 1 (from this point on, the subscript “*p*” will denote the probe beam, and the subscript “*e*” will stand for the excitation beam). The optimization of the spectrometer geometry for accounting convection processes or the Soret effect was out of the scope of this work. Quartz cells with optical path lengths of 10 mm were used throughout.

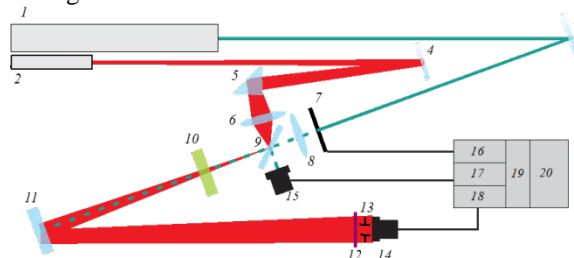


Fig. 1. Schematics of the thermal-lens spectrometer. 1 – excitation laser; 2 – probe laser; 3, 4, 9, 11 – diachronic mirrors; 5 – quartz prism; 6 & 8 – focusing lenses; 7 – chopper; 10 – sample; 12, 13 – filter and pinhole; 14, 15 – photodiodes; 16, 17, 18 – analog amplification units; 19 – DAC-ADC board; 20 – PC.

Table 1. The key parameters of the thermal lens spectrometer

Excitation Ar <sup>+</sup> laser Innova 90-6 (Coherent, USA)	Wavelengths, $\lambda_e$  Max power (TEM <sub>00</sub> mode), $P_e$ Waist, $\omega_{0e}$	514.5 and 488.0 nm  1.5 W 61.2 $\mu$ m
Probe He-Ne laser HRP020 (ThorLabs, USA)	Wavelength, $\lambda_p$ Power (TEM <sub>00</sub> mode), $P_p$	632.8 nm  2 mW
Chopper repetition rate	$\phi$ , Hz	0.1–100

### Photothermal microscope

The setup was built using an Olympus IX81 inverted microscope platform (Olympus America, Center Valley, PA), and a tunable pulsed optical parametric oscillator (Opolette HR 355 LD, OPOTEK, Inc., Carlsbad, CA) with the spectral range, 400–2200 nm; pulse width, 5 ns; pulse repetition rate, 100 Hz; and energy fluence range, 0.1–10<sup>4</sup> mJ/cm<sup>2</sup> [22]. For PT measurements, we used achromatic objectives (100× DPlan, oil, NA 1.25 and 40× PlanApo N, NA 1.42), for PA measurements (10×), all objectives from Olympus America). PT/PA imaging of the sample was implemented by sample-scanning with a two-dimensional (X-Y) translation stage (H117 ProScan II, Prior Scientific, Inc.) with a positioning accuracy of 50 nm.

In PT thermal-lens mode, laser-induced temperature-dependent variations of the refractive index (thermal lens) upon absorption of the pump laser radiation caused the defocusing of a collinear He-Ne laser (model 117A, Spectra-Physics, Santa Clara, CA) probe beam with wavelength of 633 nm and power of 1.4 mW. A decrease in the beam intensity at its centre (referred as PT signal) was detected by a photodetector with a built-in preamplifier (PDA36A, 40 dB amplification, ThorLabs, Newton, NJ) after transiting a narrow-bandpass filter (MaxLine® laser clean-up filter, central wavelength 633 nm, spectral bandwidth 12.5 nm, LL01-633-12.5, Semrock, Inc., Rochester, NY).

PT/PA imaging had a maximum positioning accuracy of 50 nm. In the linear mode, PT signal showed a linear component from fast heating (0.1–0.5  $\mu$ s) and slower (0.5–1  $\mu$ s) cooling component. In the nonlinear mode, the local temperature exceeding nanobubble-formation threshold provides an ultra-fast, sharp change in the probe beam intensity [23]. In PA mode, the laser-induced ultrasound waves were detected in a transmission configuration by focusing an ultrasound transducer (V-324-SE, 25 MHz; focal length 12 mm,

Panametrics) immersed into the ultrasonic gel above the sample.

### Other instruments

The investigations by dynamic light scattering were made using a Malvern «Zetasizer nano ZS» instrument, a He-Ne laser with 4 mW power and  $\lambda = 633$  nm. The particle size is 0.6 nm – 6  $\mu$ m. Spectrophotometric measurements were made using a Shimadzu UV-mini 1240 spectrophotometer. Ultrasonic treatment was used with a piezoceramic emitter without a concentrator immersed in the solution. The resonance frequency ~18–20 kHz, power up to 1 kW, volume 50–150 mL.

### Data treatment

A single measurement of the time-resolved PT signal  $\mathfrak{I}(t)$  for a shutter on-off cycle of the CW excitation beam and pulsed beam was calculated as the phase shift in the probe beam wavefront  $\Phi$  at a distance from a laser source  $z$  and a distance from the beam center  $r$  at time  $t$

$$\Phi = \frac{2\pi}{\lambda_p} l \frac{dn}{dT} [\Delta T(r, z, t) - \Delta T(0, z, t)] \quad (1)$$

( $\lambda_p$  is the probe laser wavelength,  $l$  is sample path length,  $dn/dT$  is the temperature coefficient of the refractive index, and  $\Delta T$  is a photothermal temperature change) as a relative change in the probe-beam intensity

$$\mathfrak{I}(t) = \left( I_p(0) - I_p(t) \right) / I_p(0)$$

As [24].

$$\mathfrak{I}(t) = 4 \left( P_e / \omega_{0e}^2 \right) \cdot B(t) \cdot E_0 D_T \cdot \alpha l = P_e \cdot B(t) / t_c \cdot E_0 D_T \cdot 2.303 \varepsilon l c \quad (2)$$

where  $I_p(0)$  is the intensity of the probe beam at the photodetector plane in the central part of the beam at the time  $t = 0$ , and  $I_p(t)$  is the intensity of the probe beam at the moment  $t$ ,  $P_e$  is the excitation laser power,  $\omega_{0e}$  is the excitation beam waist radius,  $B(t)$  is the time-dependent geometrical constant of the optical scheme,  $D_T$  is thermal-diffusion coefficient,  $\alpha$  is the linear absorption coefficient of the sample,  $\varepsilon$  is the molar absorptivity,  $c$  is molar concentration of the absorbing substance in the sample. The factor  $E_0$  is the enhancement factor of PT thermal-lens effect for unit excitation (pump) laser power

$$E_0 = (-dn/dT) / \lambda_p k, \quad (3)$$

where  $k$  the thermal conductivity. The  $t_c$  is the characteristic time of the thermal lens [24]:

$$t_c = \omega_{0e}^2 / 4D_T, \quad (4)$$

For steady-state measurements in a cw mode, (2) converts to

$$\theta = 2.303E_0P_e\epsilon lc. \quad (5)$$

Where  $\theta$  is steady-state PT signal corrected for the geometry constant  $B(t \rightarrow \infty)$ . The experimental values of the PT signal  $\theta$  were corrected to take into account a decrease in the excitation power due to light-scattering losses  $A_s$  in solutions:

$$q_{corr} = \alpha(A + A_s)/A, \quad (6)$$

where  $A$  is sample absorbance. The recalculation of the absorbance from photothermal measurements ( $A_{PT}$ ) were calculated from the equation deduced from (2) and the Beer's law  $A = \epsilon lc$

$$A_{PT} = \theta_{corr}/2.303E_0P_e. \quad (7)$$

Whenever possible, the experimental values of sample absorbance  $A_{exp}$  were corrected to scattering

$$A = A_{exp} - A_s \quad (8)$$

### Reagents and solvents

All the reagents and solvents used in this study were of cp grade or higher. Water from a Milli Q water purification system (Millipore, France) was used: pH 6.8; specific resistance 18.2 M $\Omega$ ×cm, Fe, 2 ppt; dissolved SiO<sub>2</sub>, 3 ppb; total ion amount, < 0.2 ppb; TOC, < 10 ppb. The glassware was washed with acetone followed by conc. nitric acid.

Commercially available NDs were used throughout. Trademarks, their ID labels and manufacturers are listed in Table 2. All NDs are dry powders except SDND material (already an aqueous dispersion). The aqueous dispersions were produced as reported elsewhere [25].

Table 2. Nanodiamonds used in the study

ID	NS trademarks and descriptions	Manufacturer
RUDDM	modified nanodiamond material of RUDDM grade, fraction 0–150	«Real-Dzerzhinsk» Ltd., Dzerzhinsk, Russia
SDND	Single-Digit Nanodiamonds	PlasmaChem GmbH, Germany
NanoAmando	Dispersed single-nano diamond particles NanoAmando®	NanoCarbon Research Institute Co., Ltd., Japan
GO (UDA-GO-SP)	Ultradisperse diamond UDA-GO-SP	JSC «SINTA», Minsk, Republic of Belarus



Fig. 2. Prepared aqueous dispersions of fullerenes C<sub>60</sub> (leftmost and third from the left) and C<sub>70</sub> (second from the left and rightmost), two left solutions correspond the maximum concentrations, right solutions are 10-fold diluted.

Aqueous solutions of fullerenes (Fig. 2) were produced by the following procedure. A weighed portion of fullerene (0.2–0.3 g) was placed in a 200-mL volumetric flask, dissolved in 100 mL of toluene and was sonicated for 30 min, next the solution was diluted to the mark with toluene. Next, the prepared toluene solution of the test fullerene was placed into a conic flask and 1 L of MilliQ water was added, and the solution was sonicated for 20 days (12 h per day at the maximum ultrasound power at 353K until complete evaporation of toluene (checked using HPLC-MS)). Next, the solution was boiled for 15 min and filtered through a Shott filter followed by a 0.45  $\mu$ m microporous filter. The concentration of fullerene (about 500 mg/L) was measured by determining total organic carbon (TOC) technique.

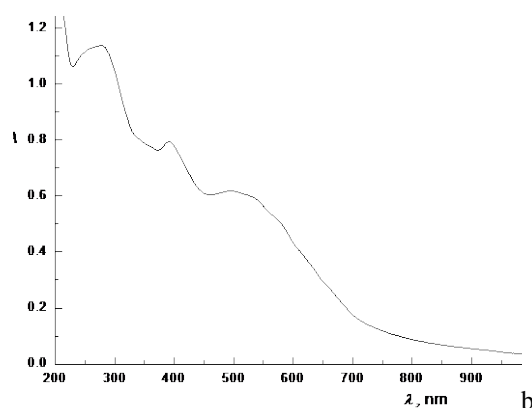
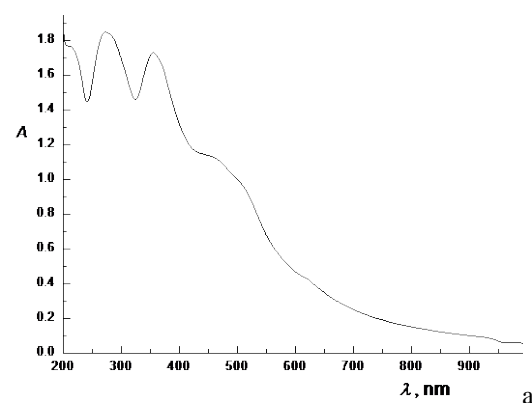


Fig. 3. Photometric spectra of prepared aqueous dispersions of fullerenes (a) C<sub>60</sub> and (b) C<sub>70</sub>.

## Results and Discussion

To date, we have worked out a novel technique for making aqueous fullerene dispersions and quantified the residual organic solvent. In development is the procedure for preparing aqueous dispersions with certain fullerene cluster sizes without organic solvents. We expect even a wider use of our findings, as many these patterns are valid also for other nanosystems such as promising nanodiamonds.

### *Sensitivity of determination of fullerenes and nanodiamonds by photothermal techniques*

Limiting absorbance detection for TLS is  $10^{-8}$  against  $10^{-5}$  for the best spectrophotometer. Dependence of steady-state thermal lens signal from concentration for fullerene C<sub>60</sub> benzene solution. Detection limit is 100 ng/ml in visible area (532 nm) and less than 1 ng/ml in UV area. The values for C<sub>70</sub> are the same. For aqueous solutions, we selected the wavelength of 488.0 nm as it corresponds to the charge-transfer complex of fullerenes in water and thus can be used for monitoring the changes in the fullerene species by its characteristic peak. The determination of aqueous dispersions of fullerene showed good linearity at  $\lambda = 488.0$  nm, and excitation power of 25 mW, the calibration plot of thermal-lens signal (Eq. (5)) on absorbance is  $\theta = (3.2 \pm 0.1)$ ,  $A - (0.01 \pm 0.01)$ , ( $P = 0.95$ ,  $n = 11$ ,  $r = 0.9903$ ). The limit of detection is 100 ng/mL for both fullerenes C<sub>60</sub> and C<sub>70</sub>, which is approximately an order lower than for spectrophotometry.

For nanodiamonds, their aqueous samples obey the Beer law. Limits of detection of all the studied nanodiamond types by thermal lens (488 nm,  $l = 1.0$  cm) are at subnanogram level (for excitation power 150 mW), which is 20-fold lower than for spectrophotometry.

Thus, for both fullerenes and nanodiamonds in their aqueous dispersions, the sensitivity of determination is rather high and comparable to the performance parameters for commonly used analytes [26]. This can be accounted for by the fact that the ND spectra are mainly absorbance. Moreover, the sensitivity of ND determination is enough for measuring low amounts of NDs (clusters) in solution. Thus, the use of photothermal microscopy is highly expedient.

### *Time-resolved photothermal measurements*

The dependence of the probe beam intensity from time (time-resolved signal) is the very rich resources of sample information. Time-resolved

thermal-lens curve depend from thermo-optical parameters (thermal conductivity, thermal capacity, thermal diffusivity,  $dn/dT$ ) of the sample, its absorption and device geometry. All of this provides a change in the measurement conditions to obtain necessary characteristics.

We investigate fullerene C<sub>60</sub> solutions in toluene (no aggregate formation, molecular solutions), in N-methylpyrrolidone (NMP), in which C<sub>60</sub> aggregates and in water (aggregates are formed and they are stabilized by charge-transfer complex). The aggregation and stabilization processes change thermo-optical parameters of solution (Eqs. (3) and (4), see Figs. 4–6).

In toluene (Fig. 4), the transient curves, Eq. (2) for fullerene C<sub>60</sub> and a molecular dye of the approximately the same molecule size (1 nm) are nearly identical. This correlates well with the theory of thermal lensing, the estimation of the characteristic time of thermal lensing  $t_c$  (Eq. (4)) shows the values for fullerene and the dye differ insignificantly from one another and from the value calculated using the reference data for toluene [21].

In NMP (Fig. 5), the situation changes drastically: the curve for fullerene goes slowly and differs from the characteristic curve of a molecular dye. This is accounted for by the formation of a coarse dispersion of fullerene in NMP, which significantly decreases the rate of heat propagation from a laser to the solution body. This is confirmed by the same effect of the second part of the curve (dissipation after the chopper switches off the excitation beam). The estimation of the cluster size is 200–300 nm.

In water (Fig. 6), the result is contrary to the previous case of NMP, the curve for a fullerene solution shows lower characteristic time than a molecular solution of a dye (ferroin), a quicker decrease in the probe laser intensity due to thermal-lens effect. This can be attributed to the formation of a finely dispersed solution of the fullerene with a cluster size of 30–50 nm [27], which exhibits a short overheating near the clusters followed by a longer period of thermal equilibrium in the whole solution [28]. It is interesting that the behavior of the dissipation part of the curve is nearly the same as for molecular dye, which is contrary to the behavior of the ND dispersions (see below).

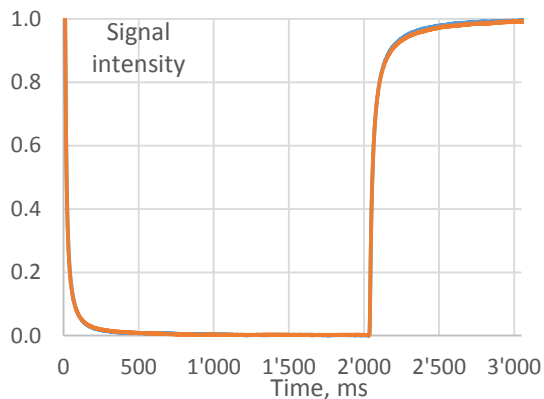


Fig. 4. Transient thermal-lens curves for fullerene  $C_{60}$ , blue line and a molecular dye (Sudan) in toluene, orange line; 532 nm, 150 mw

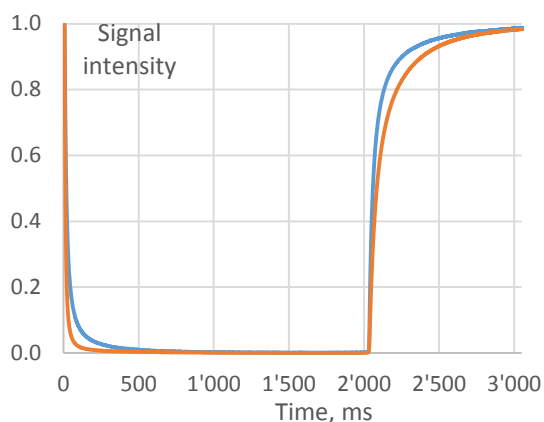


Fig. 5. Transient thermal-lens curves for fullerene  $C_{60}$ , blue line and a molecular dye (ferroin) in N-methylpyrrolidone, orange line; 532 nm, 150 mw

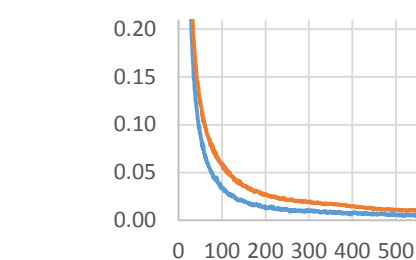
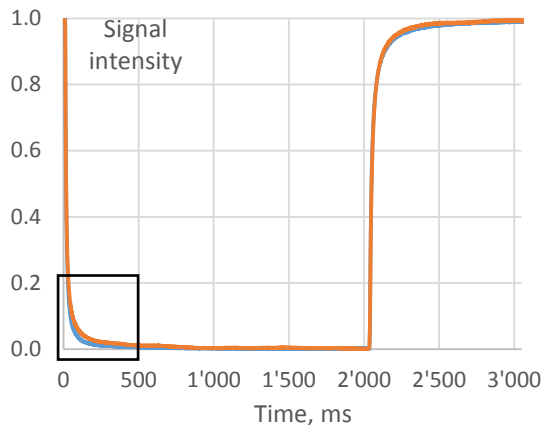


Fig. 6. Transient thermal-lens curves for fullerene  $C_{60}$ , blue line and a molecular dye (ferroin) in water, orange line; 532 nm, 150 mw. The rectangular area is expanded below

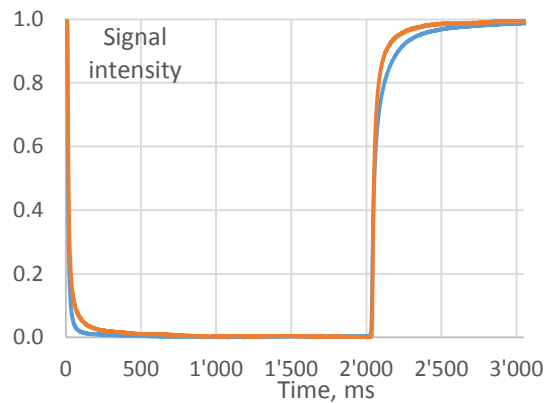


Fig. 7. Transient thermal-lens curves for ND (1.0 mg/mL, NanoAmando), blue line and a molecular dye (ferroin) in water, orange line; 532 nm, 150 mw.

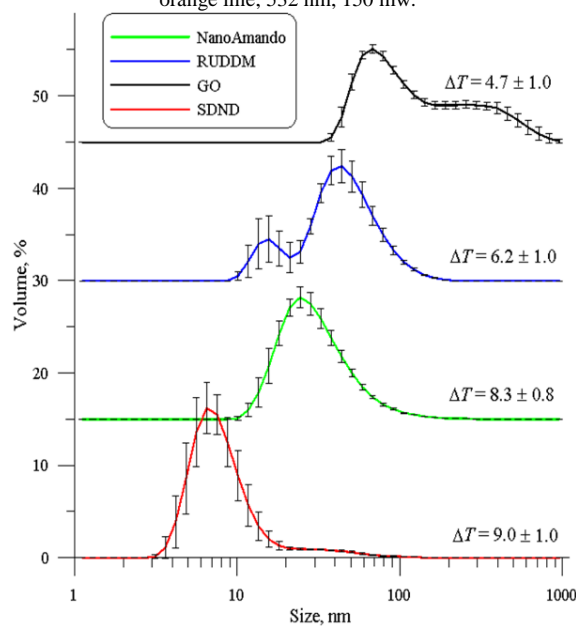


Fig 8. DLS size distributions and DSC parameter  $\Delta T$  for pristine SDND, NanoAmando, RUDDM and GO. NDs concentrations in solutions were 1.0 mg/ml (except GO solutions, 0.2 mg/ml).

The generally similar picture is observed for nanodiamond solutions (Fig. 7). This gives us the estimation of ND cluster size of 50–70 nm. From approximation of thermal-lens experiment, the estimation of aggregate size was obtained for all the types of ND used. This values correlate well with light scattering data (Fig. 8).

Unfortunately, the theory, which binds the size and the nature of the disperse particles and the behavior of the transient curve is still not fully developed, and only the estimation of the range of the particle/aggregate/cluster size can be done.

#### ***Photothermal and optoacoustic spectra of aqueous dispersions of carbon nanomaterials***

One of the drawbacks of photothermal spectroscopy to date was the limited and small number of excitation lines used for measurements. This limits the information gathered by photothermics

compared to photometry. The appearance of optical parametric oscillators (OPO) as excitation sources in laser spectroscopy fills this gap and opens up new possibilities for photothermal spectroscopy [22, 29-32], especially in biological studies. In this paper, we used OPO-based multiwavelength photothermal and optoacoustic spectroscopy for studying extinction spectra of carbon nanomaterials, as the nature of spectra (mainly absorption or mainly scattering) is still under question and conventional spectroscopic techniques (spectrophotometry and turbidimetry) cannot provide the reliable information.

The measurements of photothermal and optoacoustic spectra of the aqueous dispersions of the selected ND types (Fig. 9) shows that that absorbance calculated from OA data differ insignificantly from the conventional spectrophotometry. Photothermal-lens data are the same (not shown). As both OA and thermal lensing are much less dependent on light scattering, such a correlation of OA and conventional spectra can reveal that the spectra on nanodiamond, thought similar in shape to light scattering are determined by light absorption of these aqueous dispersions.

This confirms high sensitivity of photothermal-lens determination of nanodiamond in the visible range discussed above, which is comparable by mass limits of detection with most molecular dyes in water.

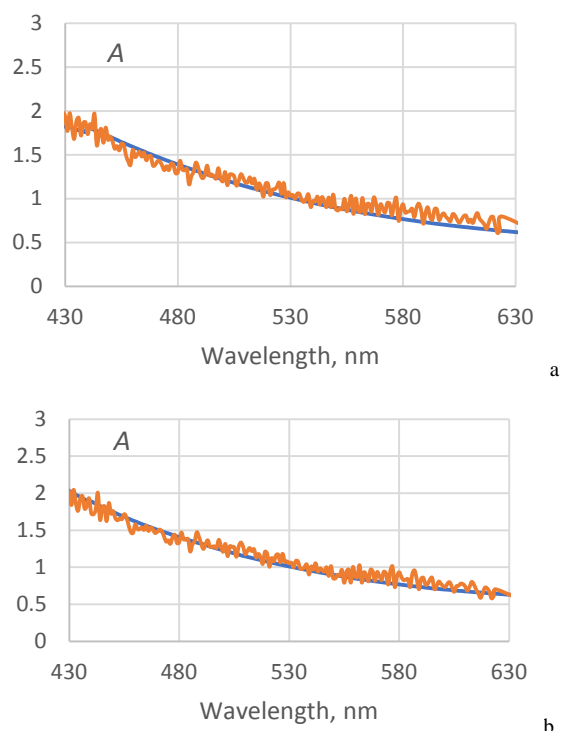


Fig. 9. Absorbance spectra of ND obtained using conventional spectrophotometry (blue lines) and calculated from optoacoustic measurements (orange lines); (a) RUDDM type; (b) SDND type.

### Photothermal and optoacoustic images of aqueous dispersions of carbon nanomaterials

The comparison of optoacoustic images of ND aqueous dispersions showed negligible differences from optical spectra of NDs thus proving the major role of absorption in their optical spectra, discussed in the previous section. Optical transmission shows no characteristic features (fig. 10), and phase-contrast images shows only disperse nature of the samples without any quantitative data.



Fig. 10. Transmission (left parts of the images) and phase-contrast (right parts) optical microscopic images of NanoAmando and RUDDM nanodiamonds (of the same ND sample).

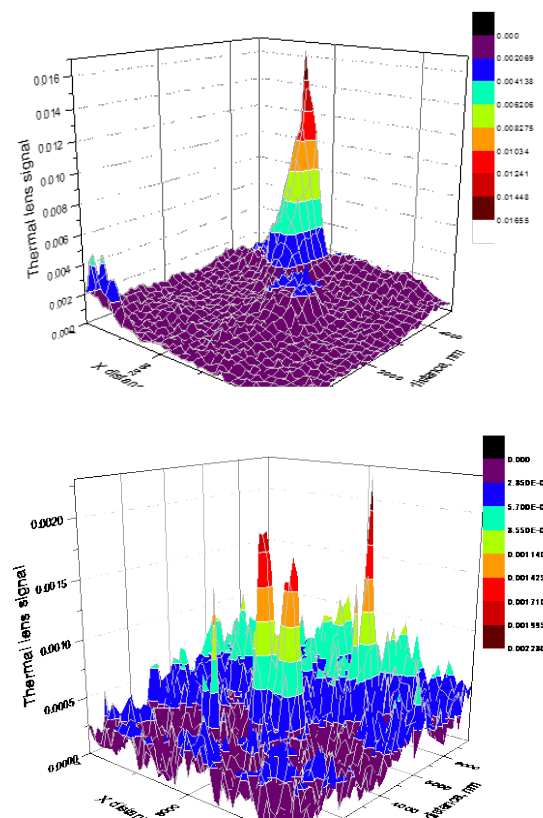


Fig. 11 the photothermal-lens microscopic images of (above) NanoAmando and (below) RUDDM nanodiamonds (532 nm, step 200 nm)

To the contrary, photothermal imaging reveals ND clusters of *ca.* 50–200 nm in ND aqueous dispersions can be revealed (Fig. 11). This is in good accordance with the data from the transient curves.

It is shown that the selected ND types differ very significantly. While SDND type show no signal at all (empty images, not shown in Fig. 11), NanoAmando ND show scarce large clusters

approximately 30–40 nm in size, RUDDM ND show much larger number of larger (50-70 nm) but lowly absorbing clusters and smaller (below 20 nm) but highly absorbing clusters. This is in good correlation with DLS distributions shown in Fig. 8.

As with transient curves discussed above, the approximation of the cluster size is rather rough as here we are limited by the optical resolution of the microscope. However, the resolution of PT microscopy can be further increased by thermal super-resolution of heat distribution during the development of the thermal lens effect [29, 33, 34].

### Conclusions

Thus, this study intended as a survey of the possibilities of photothermal and optoacoustic spectroscopy for the investigation of nanomaterials shows rather positive results. All the variants used give complementary information, and PT/OA spectroscopy can be used, along with the data from other methods, to characterize and monitor carbon nanomaterials and their promising aqueous dispersion. In our opinion, the estimation of the cluster size from two techniques—transient and imaging—giving concordant values and agreeing with DLS data are very invigorating. Although both techniques are currently unable to provide the information with enough precision due to undeveloped models, this direction of the unraveling photothermal spectroscopy shows very good outlooks.

The possibility of multiwavelength (multispectral) OPO-based photothermal techniques to complement the conventional spectrophotometric data on the nature of extinction spectra of carbon aqueous dispersions also seems very important as it can be used (with NDs, fullerenes and dispersions of various nature) to distinguish between real light absorption of these materials, light-scattering contribution, and photothermal effect to the overall picture of their properties. This seems important, even more, for biological applications of carbon nanomaterials.

### Acknowledgements

This work was supported by the Russian Foundation for Basic Research, grants nos. 10-02-01354-a, 10-03-01018-a, 12-03-00653-a, 12-03-31569-mol\_a and the Ministry of Science and Technology of Russian Federation, contract no. 16.740.11.0471.

### References

[1] D. Ho (Ed.), *Nanodiamonds: Applications in Biology and Nanoscale Medicine*, Springer, New York, Dordrecht, Heidelberg, London 2010.

- [2] O.V. Turova et al (2011), Palladium supported on detonation nanodiamond as a highly effective catalyst of the C = C and C C bond hydrogenation, *Catalysis Communications*, 12, 577-579.
- [3] N.N. Vershinin et al (2011), Detonation Nanodiamonds as Catalyst Supports, *Fullerenes Nanotubes and Carbon Nanostructures*, 19, 63-68.
- [4] V.S. Bondar, I.O. Pozdnyakova and A.P. Puzyr (2004), Applications of nanodiamonds for separation and purification of proteins, *Physics of the Solid State*, 46, 758-760.
- [5] H.-D. Wang, C.H. Niu, Q. Yang and I. Badea (2011), Study on protein conformation and adsorption behaviors in nanodiamond particle-protein complexes, *Nanotechnology*, 22.
- [6] N.A. Skorik, A.L. Krivozubov, A.P. Karzhenevskii and B.V. Spitsyn (2011), Physicochemical study of the nanodiamond surface, *Protection of Metals and Physical Chemistry of Surfaces*, 47, 54-58.
- [7] G.P. Bogatyreva, M.A. Marinich and V.L. Gvyazdovskaya (2000), Diamond — an adsorbent of a new type, *Diamond and Related Materials*, 9, 2002-2005.
- [8] B.R. Smith et al (2009), Five-Nanometer Diamond with Luminescent Nitrogen-Vacancy Defect Centers, *Small*, 5, 1649-1653.
- [9] N. Mohan et al (2010), Sub-20-nm Fluorescent Nanodiamonds as Photostable Biolabels and Fluorescence Resonance Energy Transfer Donors, *Advanced Materials*, 22, 843-847.
- [10] N. Mohan, C.-S. Chen, H.-H. Hsieh, Y.-C. Wu and H.-C. Chang (2010), In Vivo Imaging and Toxicity Assessments of Fluorescent Nanodiamonds in *Caenorhabditis elegans*, *Nano Letters*, 10, 3692-3699.
- [11] M. Chen, X.-Q. Zhang, H.B. Man, R. Lam, E.K. Chow and D. Ho (2010), Nanodiamond Vectors Functionalized with Polyethylenimine for siRNA Delivery, *The Journal of Physical Chemistry Letters*, 1, 3167-3171.
- [12] M. Chen et al (2009), Nanodiamond-Mediated Delivery of Water-Insoluble Therapeutics, *ACS Nano*, 3, 2016-2022.
- [13] L. Tang, C. Tsai, W.W. Gerberich, L. Kruckeberg and D.R. Kania (1995), Biocompatibility of chemical-vapour-deposited diamond, *Biomaterials*, 16, 483-488.
- [14] S. Kelly et al (2008), Patterned growth of neuronal cells on modified diamond-like carbon substrates, *Biomaterials*, 29, 2573-2580.
- [15] Y.-C. Chen et al (2010), Induction and regulation of differentiation in neural stem cells on ultra-nanocrystalline diamond films, *Biomaterials*, 31, 5575-5587.
- [16] L. Kuang-Kai and et al. (2007), Biocompatible and detectable carboxylated nanodiamond on human cell, *Nanotechnology*, 18, 325102.
- [17] K.-K. Liu, C.-C. Wang, C.-L. Cheng and J.-I. Chao (2009), Endocytic carboxylated nanodiamond for the labeling and tracking of cell division and

- differentiation in cancer and stem cells, *Biomaterials*, 30, 4249-4259.
- [18] A.P. Puzyr, D.A. Neshumayev, S.V. Tarskikh, G.V. Makarskaya, V.Y. Dolmatov and V.S. Bondar (2004), Destruction of human blood cells in interaction with detonation nanodiamonds in experiments in vitro, *Diamond and Related Materials*, 13, 2020-2023.
- [19] S. Vial et al (2008), Peptide-Grafted Nanodiamonds: Preparation, Cytotoxicity and Uptake in Cells, *ChemBioChem*, 9, 2113-2119.
- [20] D.Y. Lyon, L.K. Adams, J.C. Falkner and P.J. Alvarez (2006), Antibacterial activity of fullerene water suspensions: effects of preparation method and particle size, *Environ Sci Technol*, 40, 4360-4366.
- [21] M.A. Proskurnin et al (2011), In vivo multispectral photoacoustic and photothermal flow cytometry with multicolor dyes: A potential for real-time assessment of circulation, dye-cell interaction, and blood volume, *Cytometry Part A*, 79A, 834-847.
- [22] D.A. Nedosekin et al (2012), Synergy of photoacoustic and fluorescence flow cytometry of circulating cells with negative and positive contrasts, *J Biophotonics*.
- [23] V.P. Zharov and D.O. Lapotko (2005), Photothermal imaging of nanoparticles and cells, *IEEE Journal of Selected Topics in Quantum Electronics*, 11, 733-751.
- [24] S.E. Bialkowski, *Photothermal spectroscopy methods for chemical analysis*, A Wiley-Interscience publication, New York 1996.
- [25] D.S. Volkov, P.I. Semenyuk, M.V. Korobov and M.A. Proskurnin (2012), Quantification of nanodiamonds in aqueous solutions by spectrophotometry and thermal lens spectrometry, *J. Anal. Chem. (Russ.)*, 67, 842-850.
- [26] M.A. Proskurnin, E.S. Ryndina, D.S. Tsar'kov, V.M. Shkinev, A. Smirnova and A. Hibara (2011), Comparison of Performance Parameters of Photothermal Procedures in Homogeneous and Heterogeneous Systems, *Analytical Sciences*, 27, 381-387.
- [27] A.V. Brusnichkin, D.A. Nedosekin, M.A. Proskurnin and V.P. Zharov (2007), Photothermal lens detection of gold nanoparticles: theory and experiments, *Appl Spectrosc*, 61, 1191-1201.
- [28] A.A. Karabutov, E.V. Savateeva and A.A. Oraevsky (2001), Real-time photoacoustic monitoring of substance penetration in tissue, 61-70.
- [29] D.A. Nedosekin, E.I. Galanzha, S. Ayyadevara, R.J. Shmookler Reis and V.P. Zharov (2012), Photothermal confocal spectromicroscopy of multiple cellular chromophores and fluorophores, *Biophys J*, 102, 672-681.
- [30] E.I. Galanzha and V.P. Zharov (2012), Photoacoustic flow cytometry, *Methods*, 57, 280-296.
- [31] V.P. Zharov (2011), Ultrasharp nonlinear photothermal and photoacoustic resonances and holes beyond the spectral limit, *Nature Photonics*, 5, 110-116.
- [32] V.V. Tuchin, A. Tárnok and V.P. Zharov (2011), In vivo flow cytometry: A horizon of opportunities, *Cytometry Part A*, 79A, 737-745.
- [33] D.A. Nedosekin, M. Sarimollaoglu, J.H. Ye, E.I. Galanzha and V.P. Zharov (2011), In vivo ultra-fast photoacoustic flow cytometry of circulating human melanoma cells using near-infrared high-pulse rate lasers, *Cytometry A*.
- [34] D.A. Nedosekin, A.V. Brusnichkin, A.Y. Luk'yanov, S.A. Eremin and M.A. Proskurnin (2010), Heterogeneous thermal-lens immunoassay for small organic compounds: determination of 4-aminophenol, *Appl Spectrosc*, 64, 942-948.